REPORT DOCUMENTATION PAGE

AFRL-SR-BL-TR-99-

0008

1. AGENCY USE ONLY (Leave blank)	2. REPORT DATE	3. REPORT TYPE AND DATES COVERED

4. TITLE AND SUBTITLE
Influence of High-Amplitude Noise on Boundary-Layer Transition to Turbulence

5. FUNDING NUMBERS
GF 49620-96-1-0369

6. AUTHOR(S)
William S. Saric

7. PERFORMING ORGANIZATION NAME(S) AND ADDRESS(ES)

Arizona State University
Mechanical & Aerospace Engineering
Box 876106
Tempe, AZ. 85287-6106

8. PERFORMING ORGANIZATION REPORT NUMBER

9. SPONSORING / MONITORING AGENCY NAME(S) AND ADDRESS(ES)

Air Force Office of Scientific Research/NA

10. SPONSORING / MONITORING AGENCY REPORT NUMBER

11. SUPPLEMENTARY NOTES

12a. DISTRIBUTION / AVAILABILITY STATEMENT

12b. DISTRIBUTION CODE

13. ABSTRACT ***(Maximum 200 Words)***

This work completes a series of detailed experiments of boundary layers undergoing transition to turbulence with the major effort directed toward the most important issue facing the understanding of fundamental causes of transition, i.e., the receptivity to freestream disturbances. This problem is reviewed in detail by Saric et al. (1994). The present effort concentrates on leading-edge receptivity and receptivity of two-dimensional roughness. The effects of large-amplitude freestream noise is considered with the effort directed toward determining the limits of linear receptivity. Single-frequency and broad-band sound waves are used along with 2-D roughness elements to determine how the unstable waves are initiated. New data are presented on leading edge-receptivity that clarify some difficulties with previous experimental work. Comparisons with recent DNS are excellent. Data are also presented for nonlinear receptivity of 2-D roughness elements. It is shown that there is little difference between the single-frequency excitation and white noise in that the response is still keenly triggered by the amplitude of the individual mode. Thus a single frequency at 120 dB is more dangerous than white noise at 120 dB where the energy is distributed of many modes.

14. SUBJECT TERMS	15. NUMBER OF PAGES
Receptivity, boundary-layer stability, transition, nonlinear	25
	16. PRICE CODE

17. SECURITY CLASSIFICATION OF REPORT	18. SECURITY CLASSIFICATION OF THIS PAGE	19. SECURITY CLASSIFICATION OF ABSTRACT	20. LIMITATION OF ABSTRACT
Unclassified	unclassified	unclassified	UL

INFLUENCE OF HIGH-AMPLITUDE NOISE ON BOUNDARY-LAYER TRANSITION TO TURBULENCE

Final Technical Report

Full Award Period 6/15/96 – 7/14/98

SPONSOR AWARD # F49620-96-1-0369

Air Force Office of Scientific Research/NA

110 Duncan Ave, Suite B115

Bolling AFB, D.C. 20332

Attention:

Dr. Mark Glauser

December 1998

Submitted By

WILLIAM S. SARIC

Mechanical and Aerospace Engineering

College of Engineering and Applied Sciences

Arizona State Univesity

Tempe, AZ. 85287-6106

ABSTRACT

This work completes a series of detailed experiments of boundary layers undergoing transition to turbulence with the major effort directed toward the most important issue facing the understanding of fundamental causes of transition, i.e., the receptivity to freestream disturbances. This problem is reviewed in detail by Saric et al. (1994). The present effort concentrates on leading-edge receptivity and receptivity of two-dimensional roughness. The effects of large-amplitude freestream noise is considered with the effort directed toward determining the limits of linear receptivity. Single-frequency and broad-band sound waves are used along with 2-D roughness elements to determine how the unstable waves are initiated. New data are presented on leading edge-receptivity that clarify some difficulties with previous experimental work. Comparisons with recent DNS are excellent. Data are also presented for nonlinear receptivity of 2-D roughness elements. It is shown that there is little difference between the single-frequency excitation and white noise in that the response is still keenly triggered by the amplitude of the individual mode. Thus a single frequency at 120 dB is more dangerous than white noise at 120 dB where the energy is distributed of many modes.

NOMENCLATURE

c speed of sound [m/s]

F $= \omega / R = 2\pi f \nu / U_\infty^2$: dimensionless frequency

f dimensional frequency [Hz]

H $= \delta^* / \theta$: shape factor

K_s $= u'_{TS_I} / u'_{ac_{LE}}$: receptivity coefficient referenced to Branch *I*.

L $= \sqrt{\nu \hat{x} / U_\infty}$ length scale [m]

N $= \ln(A/A_I) = \int_{\hat{x}_I}^{\hat{x}} -\alpha_i d\hat{x}$

$p'_{ac} = \rho c u'_{ac}$: acoustic pressure

$R = (R_x)^{1/2} = U_\infty L/\nu$: boundary-layer Reynolds number

$R_x = U_\infty \hat{x}/\nu$: x-Reynolds number

U_∞ freestream velocity [m/s], (normalizing velocity)

$\mathbf{v}'$ (u', v', w') : disturbance velocity field normalized by U_∞ : chordwise, wall-normal, and spanwise directions

u'_{TS} rms amplitude of u' for T-S wave

u'_{ac} rms amplitude of u' for acousitc wave

$\hat{x}$ distance from virtual leading edge [m]

δ^* displacement thickness [m]

θ momentum thickness [m]

λ_{TS} Tollmien-Schlichting wavelength [m]

ν kinematic viscosity [m^2/s

1 INTRODUCTION

A typical turbulent flow produces skin-friction and heat-transfer levels that are an order of magnitude higher than that corresponding to laminar flow. In flight, control of skin friction is important for energy-efficient operation. In gas turbine engines, the prediction of the onset of turbulent flow is critical to being able to predict the heat transfer on turbine blades. Gas-turbine flows are characterized by high-amplitude freestream noise and turbulence in contrast to the flight environment which typically has very low turbulence levels. The gases entering an engine are compressed while staged blades and struts introduce large wakes into the flow. This high-pressure gas enters the combustion chamber where the fuel and chemical reactions introduce different types of unsteadiness in the flow. It is not clear how to define these disturbances except

to say that they can be decomposed to a vortical part (turbulence) and an irrotational part (acoustic noise).

Through the work of Kendall (1990, 1991, 1998), it is believed that the vortical parts of the freestream disturbances are the contributors to the 3-D aspects of the breakdown process while the work of Kosorygin et al. (1995) showed that the *irrotational* parts of the freestream disturbances contributed to the initial amplitudes of the 2-D Tollmien-Schlichting (T-S) waves. Under some conditions, high-amplitude disturbances do not follow the usual instability route and lead directly to transition (Morkovin 1993; Reshotko 1994). Thus, sound and turbulence present a different set of problems in the understanding, prediction, and control of transition to turbulence and, as such, require unusual experimental and computational techniques.

The process by which the disturbances are introduced into the boundary layer is called *receptivity*, a term first used by Morkovin (1969). Disturbances in the freestream, such as sound or vorticity, enter the boundary layer as small fluctuations of the basic state and excite unstable modes. The receptivity stage of the transition process is the least understood, but is extremely important because it provides the initial condition on the disturbance amplitude.

The second stage is the initial growth of these boundary-layer disturbances which can be described by *linear stability theory*; that is, the linearized, unsteady, Navier-Stokes equations. If the initial amplitudes of the disturbances are small, they will tend to excite the linear normal modes of the boundary layer. These normal modes in the case of a Blasius boundary layer are of the Tollmien-Schlichting (T-S) type. Their growth is weak, occurs over a viscous length scale, and can be modified, for example, by pressure gradients, surface mass transfer, and temperature gradients.

Since receptivity deals with the generation rather than the evolution of instability waves in a boundary layer, neither departures from the linear-mode scenario, called *bypass phenomena* (Morkovin 1993; Reshotko 1994), nor details of the transition process itself (Morkovin 1991; Saric 1996) are discussed here. To generate instability waves, energy from the long-wavelength external disturbances must be transferred to the shorter wavelength T-S waves through some kind of *local* (Goldstein et al. 1983a, 1983b, 1989; Kerschen et al. 1990; Crouch 1992a) or *global* (Crouch 1992b) flow adjustment. Fortunately, a number of unique reviews of earlier receptivity research were given recently by Choudhari and Streett (1994), Crouch (1994), Reshotko (1994), Saric et al. (1994), and Wlezien (1994). The reader is referred to these reviews and their references.

Since these reviews, papers have appeared by Breuer et al. (1996), Kobayashi et al. (1995, 1996), and Kato et al. (1997). They deal with different aspects of 3-D wave motion and nonlinearities and are discussed later.

Here we consider disturbances consisting of only plane acoustic waves. We ignore freestream turbulence and artificial disturbances within the boundary layer. Moreover, the main objective of this experiment is to isolate the influence of the leading edge on the initial amplitudes of T-S waves and to determine the limit of linear receptivity for 2-D roughness. The goal is to establish the framework for the active control of such fluid motions and to provide the initial conditions for computational and analytical modeling.

2. EXPERIMENTAL PROCEDURES

2.1 Basic State

This experimental investigation is conducted in the ASU Unsteady Wind Tunnel whose details are given by Saric (1992). The tunnel is a low-turbulence, closed-return wind tunnel with a 1.4 m x 1.4 m x 5.0 m test section. Besides a well-designed contraction cone, honeycomb, and seven screens that follow the guidelines of Reshotko et al. (1997), several features that contribute to the receptivity experiments are pointed out here. Both the motor/fan housing and the test section are independently mounted on isolated concrete foundations and are connected to the rest of the tunnel by flexible couplings. In addition, a sound-insulated wall separates the test section from the motor side of the tunnel and the plenum is lined with sound-reducing foam. Previous experiments have established ideal flow conditions for transition experiments.

The computer system at the Unsteady Wind Tunnel consists of a Sun *SPARCstation 20* Model 612MP that provides automatic speed control at either constant speed, constant reduced frequency, or constant Reynolds number. The hot wires are automatically temperature compensated on the computer using Radeztsky et al. (1993). All data acquisition is via 16-bit A/D boards operating at 100 kHz.

A 3-D traverse is mounted exterior to the test section with a 45° forward-swept, carbon-composite sting (3 mm thick) passed through the test-side window. The entire traverse system is enclosed and at the test section in order to avoid mass flow through the sting-access slot. Hot-wire probes on the sting are used for boundary-layer and freestream measurements. The range and step sizes are: streamwise x: 1250 mm, Δx = 12 μm; spanwise z: 100 mm, Δz = 2 μm; wall normal y: 100 mm, Δy = 1 μm.

The flat plate is Aluminum-Nickel alloy, 9.53 mm thick, 4000 mm long, and 1370 mm wide. It is ground flat, polished to 0.2 •m rms, and mounted vertically off-center (54:46) in the test-section approximately 782 mm from the contraction. Each end of the plate is machined with a unique leading edge. One is a 20:1 modified super ellipse (MSE) and the other is a 40:1 MSE. These shapes were used by Lin et al. (1992) and Fuciarelli and Reed (1994) and Fuciarelli et al. (1998) in a DNS of the receptivity problem. The geometry is described by:

$$\left(\frac{y}{b}\right)^2+\left(\frac{a-x}{a}\right)^m=1, m=2+\left(\frac{x}{a}\right)^2$$

where a is the major axis, b is the minor axis, and the coordinate origin is at the stagnation line. This shape eliminates the curvature discontinuity at the ellipse/flat-plate juncture and moves the minimum pressure region toward the leading edge. The ellipse is machined directly on the flat plate to ensure a smooth transition at the juncture. Without roughness, receptivity is limited to the leading edge.

A 500 mm flap with a sharp trailing edge is attached at the end of the plate and is used to control the location of the stagnation line. The flat plate has two rows of 25 static pressure ports on either side of the centerline. The pressure distribution along the plate is used in the initial stage to align the plate for Blasius flow. These measurements are supplemented by velocity-profile measurements that yield the shape factor, $H=\delta^*/\theta$ which is a more accurate means for establishing Blasius flow (Saric 1996). The flat plate is mounted in the test section at a slight angle of attack to compensate for the blockage due to the boundary-layer growth. The plate undergoes a series of fine adjustments until $H=2.59\pm0.7\%$ everywhere on the plate past Branch *I* of the neutral stability point. Because of the pressure gradient at the leading edge, the

local Blasius boundary layer will be referenced to a streamwise distance that is different than the wetted length. Comparisons are done with the theoretical Blasius flow and the location of the virtual leading edge is determined through a calculation of the momentum thickness for Blasius flow. For these experiments, the virtual origin, $\hat{x}_0$ is 50 mm from the leading edge and is calculated from $\hat{x}_0 = x - \hat{x}$ where x is the wetted length and $\hat{x}$ is the distance from the virtual origin defined by:

$$\hat{x} = \frac{\theta^2 U_\infty}{0.441\,\nu}$$

On the back side of the plate, "Velcro" strips are pasted near the pressure recovery region of the leading edge in order to fix the transition-to-turbulence location. To achieve symmetric flow, the stagnation line is moved to the leading edge by adjusting the flap while measuring the pressure differential of two static pressure ports placed on either side of the plate, 75 mm from the leading edge (i.e. in a region of measurable pressure gradient). The leading edge is then firmly secured in order to prevent acoustically-excited, leading-edge vibrations. Accelerometer measurements and remote laser-Doppler vibrometer measurements confirm this.

2.2 Disturbance State

The acoustic disturbances are introduced by a set of 9 McCauley Sound Inc. 250 mm diameter, 300 Watt speakers located on the plenum wall upstream of the honeycomb section. The sound pressure level in the test section can vary from 90 dB to 127 dB. At this upper level u'_∞ approaches $1\%U_\infty$. The incidence angle and amplitude of the sound wave are measured by 20 microphones placed in the walls at the leading-edge location. The relative phase measurements

show an essentially plane sound wave at zero incidence. Hot-wire measurements at the same streamwise location calibrated the microphones.

At a given speed, a dimensionless frequency, F, is chosen and the physical frequency f is calculated. Hot-wire position and flow-speed provide the Reynolds number. In this case,

$$F = 2\pi f\nu/U_\infty^2 \qquad \text{and} \qquad R = \sqrt{U_\infty \hat{x}/\nu}$$

where ν is the kinematic viscosity, U_∞ is the freestream speed, $\hat{x}$ is the distance from the virtual origin, and the appropriate length scale is $L = \sqrt{\nu\hat{x}/U_\infty}$. Thus the boundary-layer Reynolds number, R, is the square root of the Reynolds number based on $\hat{x}$.

2.3 Separation of the T-S wave from the Stokes wave

The typical boundary-layer hot-wire signal at the driving frequency is composed of the T-S wave, the Stokes wave within the acoustic boundary layer, and the probe vibrations. The hot-wire signals, measured directly with a narrow band-pass, produce something that does not resemble a T-S amplitude profile. Prior to Nishioka and Morkovin (1986), this was a typical measurement in the literature. For the experimental results given here, the different waves are separated using a new technique that is briefly described below.

The complex-plane signal-separation technique used in previous experiments (Saric et al. 1995) is a process that requires an extremely time-consuming data-sampling process since the method requires that hundreds of streamwise scans be taken so that one T-S wavelength is covered. Although the technique is successful, typically over 500 measurements are required to obtain a single T-S wave amplitude. This technique was rejected along with differential

microphones, multiple microphones, and adaptive filtering. Wlezien (1994) and Saric (1996) present critical reviews of these techniques.

The new technique is now implemented to measure the amplitude of the T-S wave. The technique is simple and effective and lends itself to understanding the behavior of the T-S wave. From linear theory, the maximum of the T-S wave propagates at approximately one third the speed of the freestream speed (about 1% of the speed of downstream-traveling sound wave). Therefore, a T-S wave generated by an acoustic wave will have a slower propagation speed than the freestream acoustic disturbance. Using this fact, the traveling T-S wave can be isolated from the acoustic disturbance and associated Stokes wave by sending bursts of sound into the test section. The initial sound burst is first measured and fractions of a second later after the sound wave has passed, the slower-traveling T-S wave initiated by the sound burst is measured.

Using this idea, bursts of sound are generated with a time interval between bursts long enough for the acoustically-forced T-S wave to pass the hot-wire before another sound burst is emitted. The hot-wire signals are narrow band-passed around the forcing frequency. Figure 1 shows a time trace depicting the sound-burst wave sensed by both wires and the trailing T-S wave measured by the boundary-layer wire for $R = 1140$, $F = 56\times10^{-6}$, $f = 80$ Hz, and $\hat{x} = 1.8$ m. Because the acquired data for one measurement can be quite large, a special acquisition process is implemented to simplify the signal processing and save storage space. The sound burst and the accompanying Stokes wave are not acquired on the boundary-layer wire and only the T-S wave is obtained and processed. An ensemble average of the bursts (typically 40) are taken to account for any low-frequency oscillations in the test section and to minimize error. This technique is useful for noise and large amplitude signals. Figure 2 shows a T-S wave profile

obtained with this method and its comparison with the solutions of the Orr-Sommerfeld Equation (OSE). The agreement between theory and experiment indicates we have a viable technique.

3 LEADING-EDGE RECEPTIVITY

The receptivity coefficient, K_S, is defined here as the ratio of the T-S amplitude and the acoustic amplitude as shown in Eq. (1).

$$K_S = \frac{|u'_{TS}|_I}{|u'_{ac}|_{LE}} \tag{1}$$

where the T-S wave amplitude is referenced to Branch *I* and the acoustic wave is measured at the leading edge. This particular definition is convenient for the experiments because it is almost impossible to separate and measure the embryonic T-S wave near the leading edge. However, by using linear stability theory, the result can be scaled to the leading edge and compared with receptivity theory (Goldstein 1983a; Kerschen et al. 1990).

All T-S amplitudes are measured near Branch *II* using the pulsed-signal technique (section 2.3) for different *F* and *R* combinations. Because the T-S amplitudes at Branch *I* are of the order of $10^{-6}U_\infty$ the linear growth from Branch *I* to near Branch *II* is used to amplify the signal. The amplitude near Branch *II* is of the order of $10^{-4}U_\infty$ and is then scaled to Branch *I* using the Orr-Sommerfeld equation. The freestream acoustic disturbances are measured at the leading edge with a hot wire. The receptivity coefficient is calculated from

$$K_S = \frac{|u'_{TS}|_R e^{-N}}{|u'_{\mathrm{ac}}|_{\mathrm{LE}}} \tag{2}$$

where N is the integrated growth rate from Branch I to the Reynolds number of the measurement.

3.1 Previous Results

The data of Saric et al. (1995) showed a very narrow pass-band of receptive frequencies. This was behavior not predicted by analysis (Kerschen et al. 1990) or computation (Fuciarelli and Reed 1994) and was at odds with Orr-Sommerfeld Equation (OSE) results. Krutckoff (1996) continued the measurements of this flow field and concentrated on measuring the rms of the difference of the streamwise fluctuations on both sides of the plate. Frequency sweeps demonstrated that this measurement had peaks at the same receptivity frequencies. Obviously, the continuous, phase-correlated sound signal was forcing a resonance in the wake causing an asymmetric oscillation which fed back to the leading edge in the form of fluctuations transverse to the leading edge. This obviously biased these experiments.

3.2 Present Results

As part of the new experiments, continuous white noise input was placed in the freestream. Figure 3 is a spectrum of the freestream and boundary-layer response. Superposed are the OSE calculations. The agreement between the boundary-layer response and the OSE calculations show that when the phase information is destroyed, wake resonance cannot occur and the leading-edge receptivity pass-band is congruent with the OSE pass band for T-S waves. This confirms the problems Saric et al. (1995) had with wake forcing.

Figure 4 is a summary of the results from the 20:1 leading edge at the 8 m/s condition using the pulsed sound technique. The pulsed technique essentially measures the T-S wave before the sound interacts with the trailing edge giving a band of amplified T-S waves that is broader than

Saric et al. (1995). Thus, all previous receptivity experiments need to be re-evaluated in the light of this new information.

A comparison with receptivity theory (Goldstein et al. 1983a,b, 1989; Kerschen et al. 1990) and DNS (Fuciarelli et al. 1998) is done for the case of the 20:1 MSE and $F = 84\times10^{-6}$. These conditions represent the lowest Reynolds number that can be done with the experiment and highest Reynolds number that can be handled by the DNS. Based on the scaling of the asymptotic theory, we assume that the Orr-Sommerfeld region begins around $\hat{x} \approx \lambda_{TS}/2$. The amplitude-ratio decay from this point to Branch *I* is 0.154 based on stability calculations of the basic state determined from DNS (Fuciarelli and Reed 1994). With K_S= 0.05, the receptivity coefficient, scaled to the leading edge, is 0.33 which compares with the theoretical calculations of 0.95 by Kerschen et al. (1990). Haddad and Corke (1998) did a DNS of a parabolic leading edge and obtained results more comparable with other DNS than the analysis.

The DNS of Fuciarelli et al. (1998), using the same definition of K_S as Eq. 1, show K_S= 0.048 as compared with the experimental value of 0.05 in Figure 4. The agreement is quite good and lends evidence that the pulsed technique is the only reliable method.

4 2-D ROUGHNESS RECEPTIVITY

The receptivity of 2-D roughness is done in order to extend the work of Saric et al. (1991) and Kosorygin et al. (1995) to the nonlinear sound range.

Saric et al. (1991) presented receptivity data at a fixed sound pressure level (90 dB) and showed nonlinearity with roughness height. These experiments were successfully modeled by Choudhari and Streett (1992; 1994), Crouch (1992a,b; 1994), and Nayfeh and Ashour (1994). Nayfeh and Ashour (1994) were able to show the constructive interference between the T-S wave

generated at the leading edge and the T-S wave generated at the roughness - a fact confirmed by Kosorygin et al. (1995).

Figure 5 presents T-S wave amplitude as a function of freestream sound amplitude. This is single sine-wave forcing over a 45 μm, 2-D roughness located at x = 0.62 m. Measurements taken at U_∞ = 12.75 m/s, x = 1.60 m, f = 75.8 Hz, $F = 50 \times 10^{-6}$. Conditions of Saric et al. (1991). Since large-amplitude sound in the freestream may itself contain harmonics of the fundamental, the appearance of harmonics within the boundary layer is not prima facie evidence of nonlinear receptivity. Therefore, the departure of *normalized* T-S amplitude from a constant value is the indicator of nonlinearity provided the mean boundary-layer velocity has not changed. Thus, Figure 5 shows departure from linearity at 110 dB. Also shown is the local mean boundary-layer velocity normalized with the freestream. It remains constant so the boundary layer is still laminar and hence the departure of the normalized T-S amplitude from a constant value is just nonlinear receptivity. Figure 6 has the spectra from the last three points and it is clear that the spectra are laminar.

Figure 7 is the taken under the same conditions as Figure 6 except the measurement point is x = 1.80 m. We still see departure from linearity at 110 dB but now we see the departure from laminar flow (transition) at 117 dB. Figure 8 is the corresponding spectrum of three points near the peak amplitude. Now we see a build-up of the subharmonic and a definite transitional spectrum. Breuer et al. (1996) also observed a subharmonic breakdown using sound and 2-D roughness. The data of Figs. 5-8 were taken with continuous sound and a fixed wire but they have been verified using the pulsed technique. Typically the T-S wave is so dominant with large 2-D roughness, it is not necessary to use heroic efforts to subtract the Stokes wave.

There appears to be no basic difference between broad-band and single frequency waves except that an order of magnitude increase in power is required over the broad band to achieve similar transition results of a single-frequency wave. However, the following sequence of figures (Figures 9 - 12) shows the nonlinear and transitional influence of the broad-band input.

Disturbance amplitude and mean velocity versus freestream sound pressure level are shown. White-noise forcing with 20 - 150 Hz bandpass over 45 μm, 2-D roughness at x = 0.62 m. Measurements taken at U_∞ = 12.75 m/s, x = 1.60 m. In these measurements, 2-D strips are doubled and then placed one T-S wavelength downstream. The basic roughness size is 45 μm. The use of the four types of roughness elements, (45, 0), (90, 0), (90, 45), and (90, 90) is still in the linear range since it has been shown (Crouch 1994, Kobayashi et al. 1995, 1996) that the addition of a roughness element one T-S wave downstream is linear superposition. Thus, the receptivity can be increased without approaching the nonlinear threshold of roughness height.

One can see from Figures 9-12 that the nonlinear regime of disturbance amplitude occurs at lower sound amplitude and that transition (as measured by the mean velocity) moves forward. At sound pressure levels up to 125 dB, no bypass was observed. However, the data base for the theoretical models has been enhanced for both the nonlinear onset and transition location.

CONCLUSIONS

Leading Edge Receptivity

The sharp focusing of a single acoustic wave (Saric et al. 1995) is due to complicated duct acoustics. The correct measurements are made with sound pulses that are conditionally sampled. The actual receptivity coefficients are different and more broad band - consistent with DNS and

OSE. Agreement between theory, DNS, and experiments is good when results are extended to Branch I.

Broad Band versus Single Mode

No essential difference between broad band and single mode. For a given sound pressure level, there is more energy in the single mode that and wave in the broad band. One needs a 30 dB increase in broad band to approach effects of single mode.

Nonlinearity

Leading-edge receptivity is much weaker than 2-D roughness and hence no nonlinearity is observed. Receptivity of 2-D roughness departs from linear behavior at freestream levels of 110 dB for single-mode excitation. Breakdown appears to be via a subharmonic type. No bypass observed for freestream sound levels up to 127 dB (which is the present limit of the facility).

ACKNOWLEDGMENTS

The authors would like to acknowledge the contributions of Dr. Mark Reibert during the nascent stage of this work. The continuous help and assistance of Mr. Dan Clevenger, Dr. Keith Chapman and Mr. Ian Lyttle is greatly appreciated.

This work was sponsored (in part) by the Air Force Office of Scientific Research, USAF, under *Grant Number F49620-96-1-0369.* The support of E.B.W. through the ASU University Graduate Scholar program and the Allied Signal Fellowship program is gratefully acknowledged. The acoustic speakers were donated by McCauley Sound Inc., Puyallup, Washington.

REFERENCES

Breuer, K.S., Grimaldi, M.E., Gunnarsson, J. and Ullmar, M. 1996 Linear and nonlinear evolution of boundary layer instabilities generated by acoustic receptivity mechanisms. *AIAA Paper 96-0183.*

Choudhari, M. and Streett, C. 1992 A finite Reynolds number approach for the prediction of boundary-layer receptivity in localized regions. *Phys. Fluids A,* ***4***, 2495.

Choudhari, M. and Streett, C. 1994 Theoretical predictions of boundary layer receptivity. *AIAA Paper 94-2223.*

Crouch, J.D. 1992a Localized receptivity of boundary layers. *Phys. Fluids A* ***4***, 1408.

Crouch, J.D. 1992b Non-localized receptivity of boundary layers. *J. Fluid Mech.,* ***244***, 567.

Crouch, J.D. 1994 Receptivity of boundary layers. *AIAA Paper 94-2224.*

Fuciarelli, D.A. and Reed, H.L. 1994 Direct Numerical Simulations of Leading-Edge Receptivity to Freestream Sound. *Application of Direct and Large Eddy Simulation to Transition and Turbulence, AGARD CP 551,* 29-1.

Fuciarelli, D.A., Reed, H.L. and Lyttle 1998 DNS of Leading-Edge Receptivity. *AIAA Paper 98-2644.*

Goldstein, M.E. 1983a The evolution of Tollmien-Schlichting waves near a leading edge. *J. Fluid Mech., Vol. 127,* 59.

Goldstein, M.E. and Hultgren, L.S. 1989 Boundary-layer receptivity to long-wave disturbances. *Ann. Rev. Fluid Mech., Vol. 21,* 137.

Goldstein, M.E., Sockol, P.M. and Sanz, J. 1983b The evolution of Tollmien-Schlichting waves near a leading edge. Part 2. Numerical determination of amplitudes. *J. Fluid Mech., Vol. 129,* 443.

Haddad, O. and Corke, T.C. 1998 Boundary layer receptivity to freestream sound on parabolic bodies. in press *J. Fluid Mech.*

Kato, T., Fukunishi, Y. and Kobayashi, R. 1997 Artificial control of the three-dimensionalization process of T-S waves I boundary-layer transition. *JSME Int'l J., Ser. B,* Vol. 40, No. 4, pp 536-41.

Kendall, J.M. 1990. Boundary layer receptivity to freestream turbulence. *AIAA Paper 90-1504.*

Kendall, J.M. 1991 Studies on laminar boundary-layer receptivity to freestream turbulence near a leading edge. *Boundary Layer Stability and Transition to Turbulence, FED-Vol. 114*, 23. Eds: D.C. Reda, H.L. Reed, R. Kobayashi, ASME.

Kendall, J.M. 1998 Experiments on boundary-layer receptivity to freestream turbulence. *AIAA Paper 98-0530.*

Kerschen, E.J., Choudhari, M. and Heinrich, R.A. 1990 Generation of boundary instability waves by acoustic and vortical freestream disturbances. *Laminar-Turbulent Transition, Vol. III,* Eds. D. Arnal and R. Michel, Springer-Verlag.

Kobayashi, R., Fukunishi, Y., Nishikawa, T. and Kato, T. 1995 The receptivity of flat-plate boundary layers with two-dimensional roughness elements to freestream sound and its control. *Laminar-Turbulent Transition, Vol. IV*, Ed. R. Kobayashi, Springer.

Kobayashi, R., Fukunishi, Y., Kato, T. 1996 Laminar flow control of boundary layers utilizing acoustic receptivity. *Sixth Asian Congress of Fluid Mechanics*, Singapore, Vol.1, pp 629-32.

Kosorygin, V.S., Radeztsky, R.H., Jr., and Saric, W.S. 1995 Laminar boundary layer sound receptivity and control. *Laminar-Turbulent Transition, Vol. IV*, Ed. R. Kobayashi, Springer.

Krutckoff, T.K. 1996 Experiments on boundary-layer receptivity to sound. M.S. Thesis, Arizona State University, August 1996.

Lin, N., Reed, H.L. and Saric, W.S. 1992 Effect of leading edge geometry on boundary-layer receptivity to freestream sound. *Stability, Transition and Turbulence*, eds. M.Y. Hussaini, A. Kumar, C.L. Streett Springer-Verlag, New York.

Morkovin, M.V. 1969 On the many faces of transition. *Viscous Drag Reduction* ed.: C.S. Wells, Plenum.

Morkovin, M.V. 1991 Panoramic view of changes in vorticity distribution in transition instabilities and turbulence. *Boundary Layer Stability and Transition to Turbulence, FED-Vol. 114*, 1. Eds: D.C. Reda, H.L. Reed, R. Kobayashi, ASME.

Morkovin, M.V. 1993 Bypass-transition research: Issues and philosophy. *Instabilities and Turbulence in Engineering Flows*, Eds: D.E. Ashpis, T.B. Gatski, R. Hirsh, Kluwer Academic.

Nayfeh, A.H. and Ashour, O.N. 1994 Acoustic receptivity of a boundary layer to Tollmien-Schlichting waves resulting from a finite-height hump at finite Reynolds numbers. *Phys. Fluids A* ***6***, 3705.

Nishioka, M. and Morkovin, M.V. 1986 Boundary-Layer Receptivity to Unsteady Pressure Gradients: Experiments and Overview, *J. Fluid Mech. Vol. 171.*

Radeztsky, R.H. Jr., Reibert, M.S. and Takagi, S. 1993 A software solution to temperature-induced hot-wire voltage drift. *Proc. 3rd International Symposium on Thermal Anemometry*, ASME-FED, June 1993.

Reed, H.L. 1997 Role of Direct Numerical Simulations in Transition Modeling. *(Invited) First AFOSR DNS/LES Conference*, New Orleans, August 1997.

Reed, H.L., Haynes, T.S., Saric, W.S. 1998 CFD validation issues in transition modeling. *AIAA J.*, Vol 36, No. 5, pp 742-51.

Reed, H.L., Saric, W.S. and Arnal, D. 1996 Linear Stability Theory Applied to Boundary Layers. *Ann. Rev. Fluid Mech. Vol. 28*, pp. 389-428.

Reshotko, E. 1994 Boundary layer instability, transition, and control. *AIAA Paper 94-0001.*

Reshotko, E. 1997 Flow quality issues for large wind tunnels. *AIAA Paper 97-0225.*

Saric, W.S. 1992 The ASU transition research facility. *AIAA Paper 92-3910.*

Saric, W.S. 1996 Low-Speed Boundary Layer Transition Experiments. *Transition: Experiments, Theory & Computations*. Eds. T.C. Corke, G. Erlebacher, M.Y. Hussaini, ICASE Lecture Notes. Copies are available from the author.

Saric, W.S., Hoos, J.A., and Radeztsky, R.H. Jr. 1991 Boundary-layer receptivity of sound with roughness. *Boundary Layer Stability and Transition, FED-Vol. 114*, Eds: D.C. Reda, H.L. Reed, R. Kobayashi, ASME.

Saric, W.S., Reed, H.L. and Kerschen, E.J. 1994 Leading-edge receptivity to sound: Experiments, DNS, theory. *AIAA Paper 94-2222.*

Saric, W.S., Wei, W., Rasmussen, B.K. and Krutckoff, T.K. 1995 Experiments on Leading-Edge Receptivity to Sound. *AIAA Paper 95-2253.*

Wlezien, R.W. 1994 Measurement of acoustic receptivity. *AIAA Paper 94-2221.*

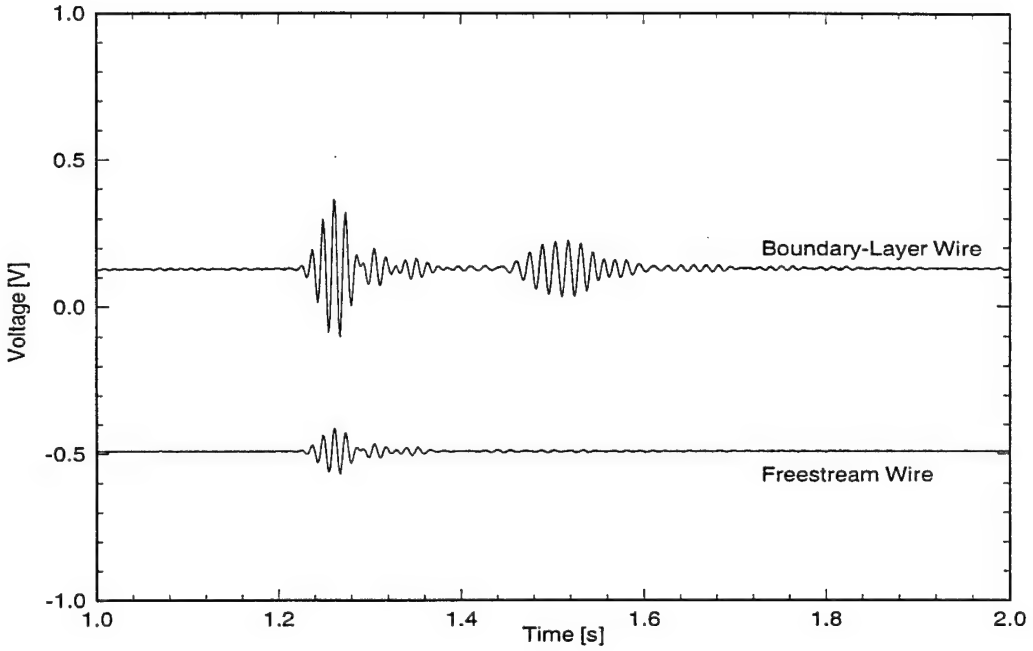

Figure 1. Time traces of freestream hot wire and boundary-layer hot wire for sound burst

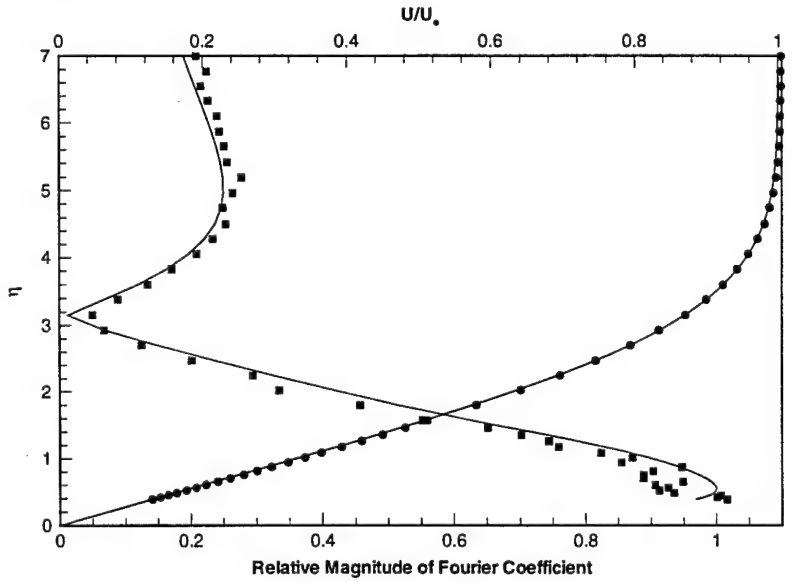

Figure 2. Comparison of measured meanflow and disturbance flow with theory. 2-D roughness at 90 μm. 100 Averages with pulsed technique. R = 1051, $F = 60\text{x}10^{-6}$

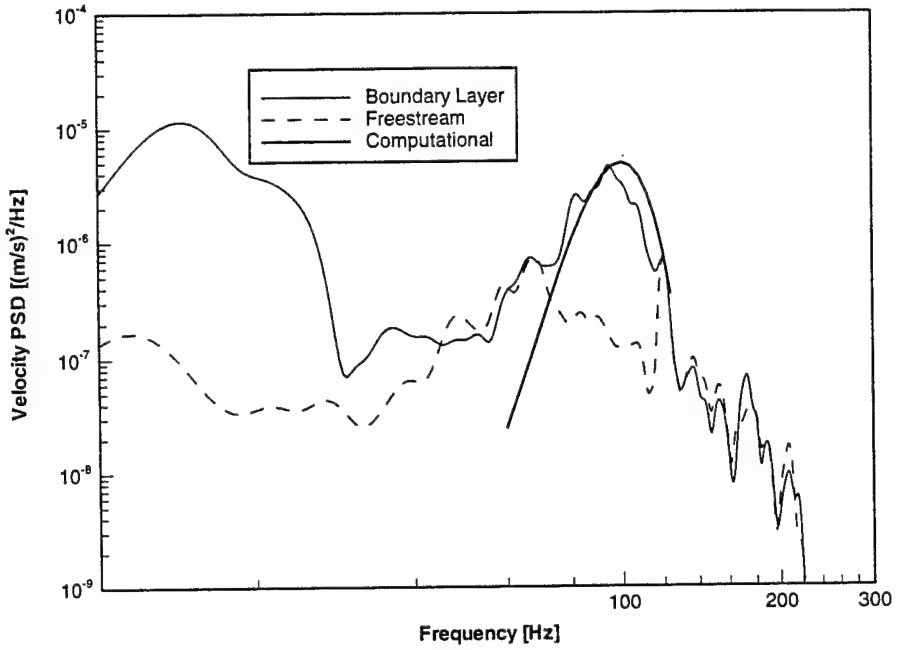

Figure 3. Specrum of white noise in freestream, boundary layer response, and the OSE spectrum. Leading edge receptivity only.

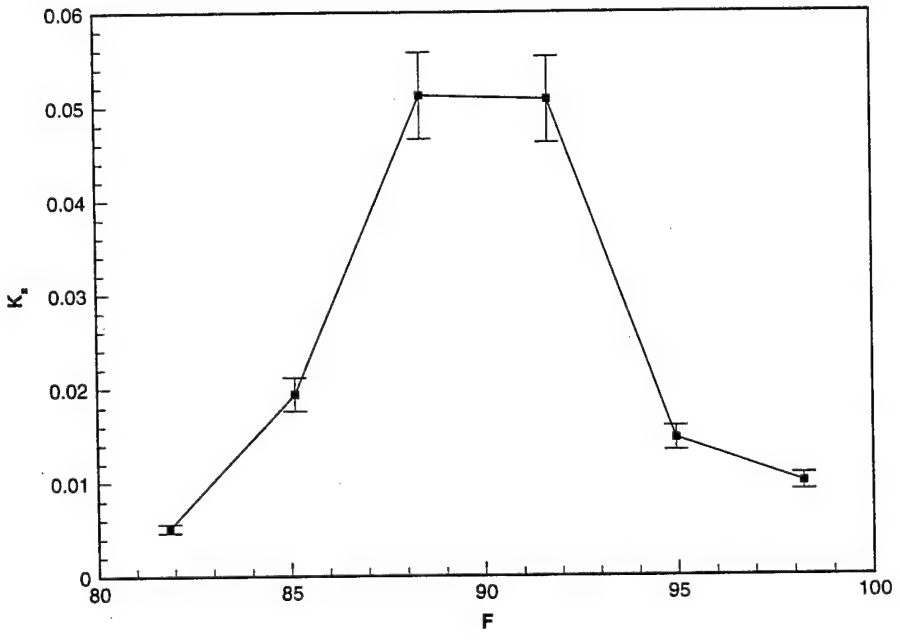

Figure 4. Receptivity coeficient, K_s, for $U_\infty = 8$ m/s.

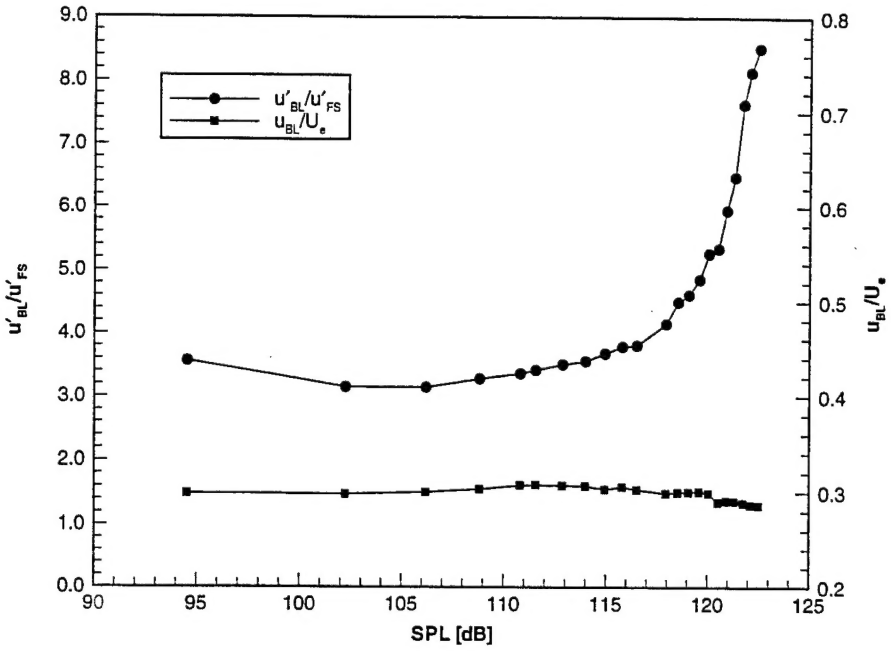

Figure 5. Disturbance amplitude and mean velocity versus freestream sound pressure level. Sine-wave forcing over 45 μm, 2-D roughness at x = 0.62 m. Measurements taken at U_∞ = 12.75 m/s, x = 1.60 m, f = 75.8 Hz, $F = 50\text{x}10^{-6}$. Conditions of Saric et al. (1991).

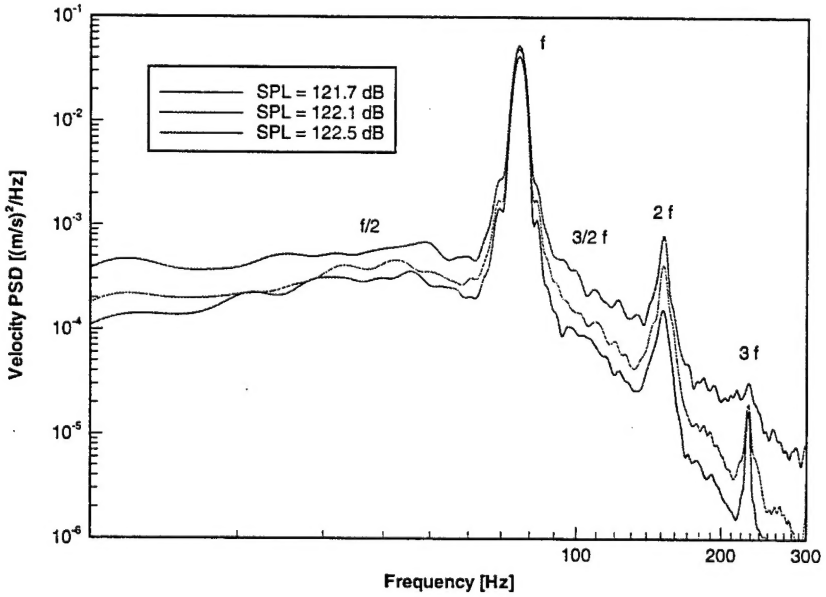

Figure 6. Spectra of the last three points of Figure 5.

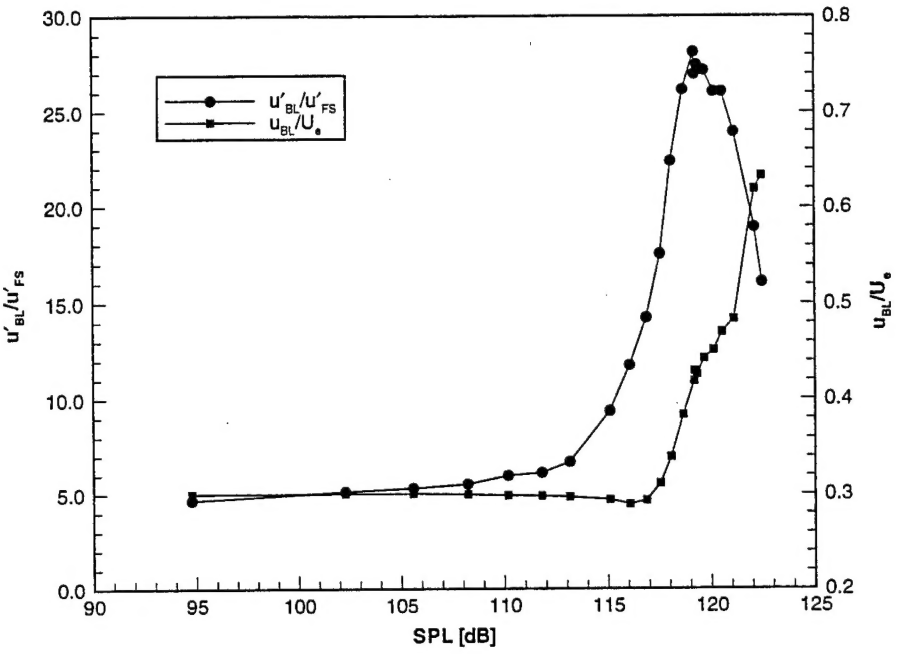

Figure 7. Same as Figure 5 except measurements taken at $x = 1.80$ m.

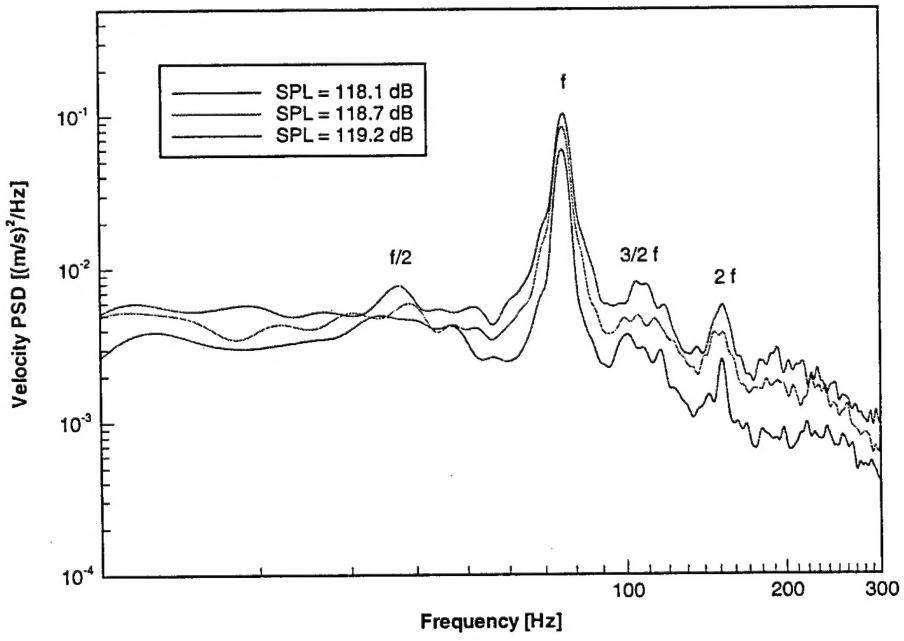

Figure 8. Spectra of three points near the maximum amplitude of Figure 7.

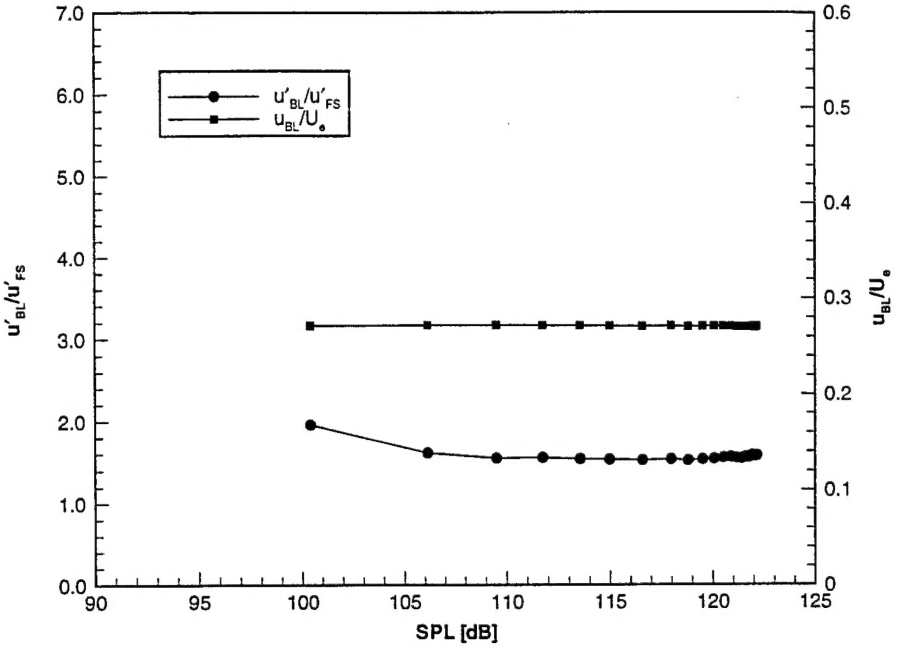

Figure 9. Disturbance amplitude and mean velocity versus freestream sound pressure level. White-noise forcing with 20 - 150 Hz bandpass over 45 μm, 2-D roughness at $x = 0.62$ m. Measurements taken at $U_\infty = 12.75$ m/s, $x = 1.60$ m.

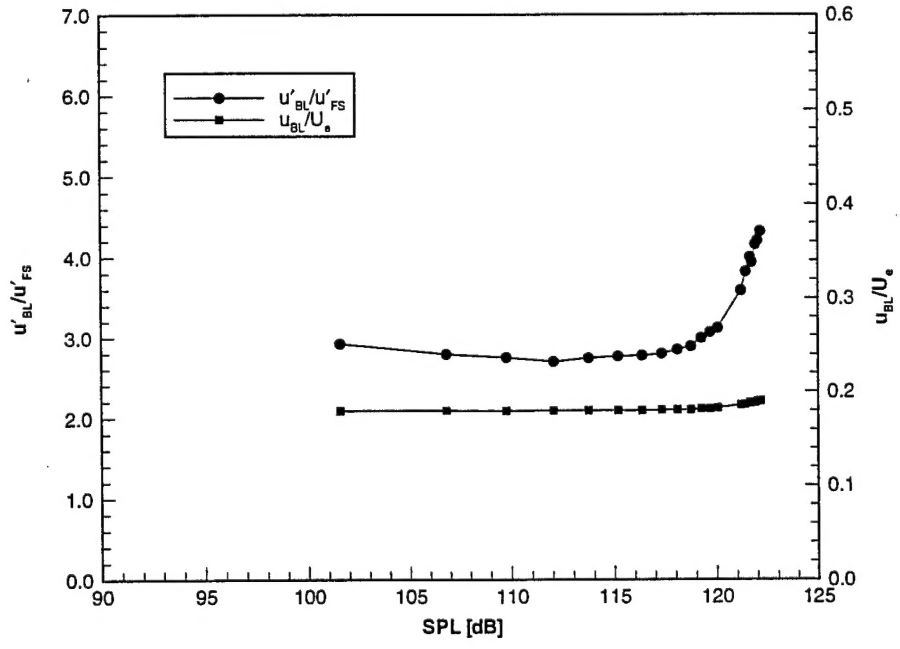

Figure 10. Same conditions as Figure 9 except 90 μm roughness at $x = 0.62$ m.

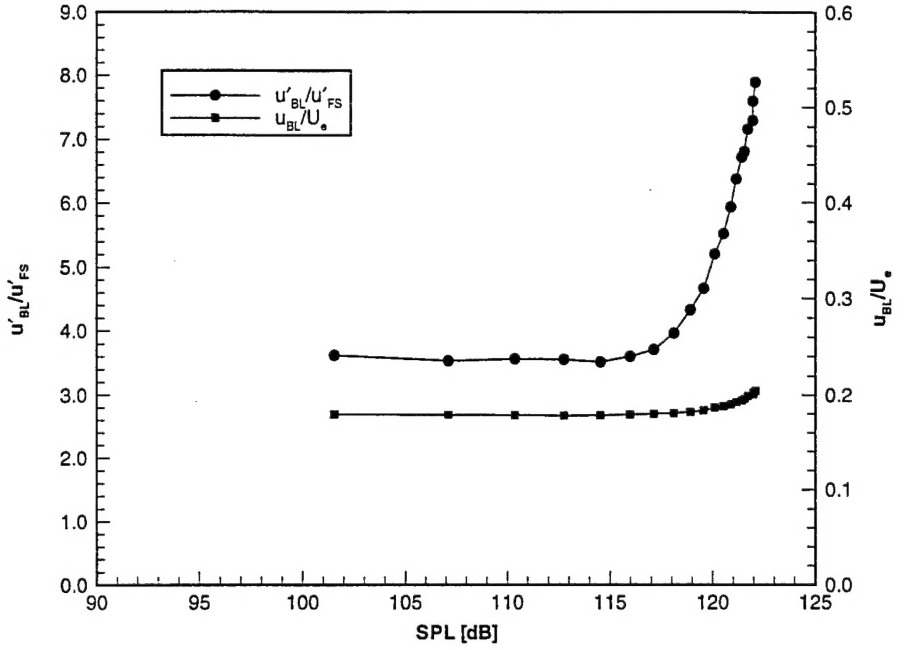

Figure 11. Same conditions as Figure 9 except 90 μm roughness at x = 0.62 m and 45 μm roughness at x = 0.67 m.

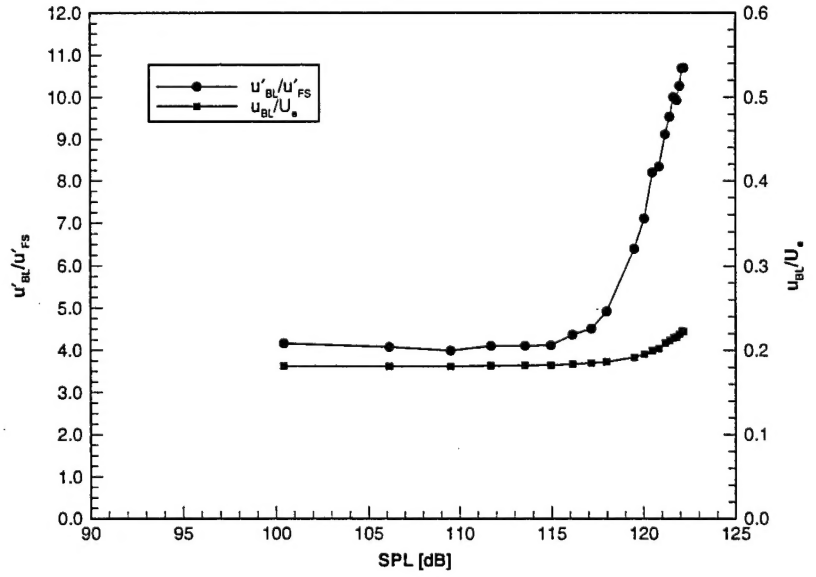

Figure 12. Same conditions as Figure 9 except 90 μm roughness at x = 0.62 m and 90 μm roughness at x = 0.67 m.